Applied Catalysis B: Environmental 147 (2014) 851–857

Contents lists available at ScienceDirect

Applied Catalysis B: Environmental

journal homepage: www.elsevier.com/locate/apcatb

Fluorine mediated photocatalytic activity of $BiPO_4$

Yanfang Liu, Yanhui Lv, Yanyan Zhu, Di Liu, Ruilong Zong, Yongfa Zhu*

Department of Chemistry, Beijing Key Laboratory for Analytical Methods and Instrumentation, Tsinghua University, Beijing 100084, China

ARTICLE INFO

Article history:
Received 3 July 2013
Received in revised form
26 September 2013
Accepted 29 September 2013
Available online 18 October 2013

Keywords:
$BiPO_4$
Fluorine doping
Photocatalysis
Enhancement
Mechanism

ABSTRACT

The fluorine doped $BiPO_4$ (F-$BiPO_4$) photocatalyst was synthesized via an in situ fluorination method. The lattice oxygen of $BiPO_4$ was substituted by fluorine, resulting in the increased polarizability and thus an increased induced dipole moment of $BiPO_4$, which can increase the separation efficiency of electron-hole pairs. The photocatalytic activity of $BiPO_4$ was enhanced by about 30% when the molar ratio of F/Bi was 0.03. Not only the discoloration rate of methylene blue (MB) but also the mineralization rates of MB and phenol were accelerated by F-doping. The enhancement of photocatalytic activity by F-doping could be attributed to the stronger adsorption ability of the substrate, the larger amount of active facet and higher separation efficiency of electron-hole pairs resulted from the increased polarizability. Overdoping would decrease the photocatalytic activity due to the increased recombination rate of electron-hole pairs at high defect concentration.

1. Introduction

$BiPO_4$ is a newly discovered photocatalyst with more attractive UV light activity than TiO_2 (P25, Degussa) [1,2] and it has attracted increasing interest in the past few years [3–9]. It is not only efficient in decoloration of dye, but also superior in mineralization of the difficult degradable phenol. Synergy of $BiPO_4$ and adequate H_2O_2 can raise the removal efficiency of phenol greatly [10]. Therefore, $BiPO_4$ is a promising photocatalyst and has much potential in remediation of environment. However, similar to TiO_2, $BiPO_4$ is also a wide band gap (ca. 3.85 eV) photocatalyst and the quantum efficiency is not high enough to meet the requirement of industrial application. Thus, it still needs to improve the photo-performances of $BiPO_4$ photocatalyst. How to increase its quantum efficiency and extend its light absorption range?

Doping is one of the methods to modify the bulk and surface characteristics and thus the light absorption range as well as the photocatalytic activity [11]. Both metal and nonmetal doping, as well as co-doping [12] have been investigated, and there are many excellent reviews related to doping [13,14]. Although cationic metal doping can induce a red shift in the band gap transition and may enhance the photocatalytic activity under both UV and visible light, some cationic metal dopants may also serve as recombination centers for photogenerated charge carriers and result in reduced photocatalytic activity [14]. Anionic nonmetal doping such as C [15], N [16,17], P [18], S [19,20], F [21–25], I [26] seems to be more efficient and it is proved to have narrowed the band gap or improved the photocatalytic activity of different photocatalysts by inducing impurity states, which are supposed to be close to the valence band maximum. This can not only narrow the band gap, but also increase the separation efficiency of electron-hole pairs and thus the photocatalytic activity. Among the anionic nonmetal dopants, fluorine is investigated most extensively and has been demonstrated to improve the photocatalytic activity of TiO_2 [25,27,28] and non TiO_2-based photocatalysts [22,24,29–31]. Whether the photocatalytic activity can be improved and how much it can be improved by F-doping largely depend on the chemical nature of incorporated fluorine (such as adsorbed fluoride and lattice-doped fluorine) and the fluoride-mediated crystal modification and organization. Surface-fluorinated TiO_2 has been proved to be an effective surface modification method to improve its UV light photocatalytic activity [32], but it cannot induce strong visible light absorption [23]. Interestingly, Xing et al. [33] used a special structure of supported mesoporous catalyst to facilitate the surface fluorination of TiO_2, and it was found that the surface fluorination enhanced the UV light photocatalytic activity and together with the Ti^{3+} generation led to the excellent adsorption capacity and visible light photocatalytic activity of TiO_2. Lattice-doped fluorine can efficiently improve the photocatalytic activity [22,29] and sometimes can induce a red shift of the optical absorption edge of composite oxide photocatalyst [30]. For example, the fluorine interstitially doped $ZnWO_4$ can induce the distortion of WO_6 octahedron, resulting in an enhanced internal electric field and then an increased transfer rate of photogenerated electrons and holes to the catalyst surface, and thus an enhanced photocatalytic activity for degradation of Rhodamine B (RhB) and 4-chlorophenol (4-CP)

* Corresponding author. Tel.: +86 10 62787601; fax: +86 10 62787601.
E-mail address: zhuyf@tsinghua.edu.cn (Y. Zhu).

0926-3373/$ – see front matter © 2013 Elsevier B.V. All rights reserved.
http://dx.doi.org/10.1016/j.apcatb.2013.09.050

[22,29]. Similar promotion in the photocatalytic activity over F-doped Bi_2WO_6 was also reported [24]. Is it possible to improve the photocatalytic activity of the excellent UV light responsive $BiPO_4$, and further induce its visible light photocatalytic activity by F-doping? This is an inviting question and deserves intensive investigation.

The present work intends to explore the preparation and performance enhancement of F-$BiPO_4$. The effects of fluorine on the crystal structure and photocatalytic activity of $BiPO_4$ have been investigated. Besides, detailed mechanism for the improved photocatalytic activity by F-doping has been discussed.

2. Experimental

2.1. Preparation and characterization of F-$BiPO_4$ photocatalysts

$BiPO_4$ and F-$BiPO_4$ were synthesized via a hydrothermal process. All chemicals used were analytic grade reagents. In a typical procedure, 8 mmol of $Bi(NO_3)_3{\cdot}5H_2O$ and 160 mL distilled water were put into a beaker under magnetic stirring. Then 28.8 mmol $NaH_2PO_4{\cdot}2H_2O$ and certain amount of NaF were added into the mixture and stirred for 1 h. The resulting suspension was transferred into a Teflon-lined stainless steel autoclave and maintained at 160 °C for 24 h. The products were washed three times with distilled water and dried at 120 °C for 8 h.

The products were characterized by X-ray diffraction (XRD) on Bruker D8-advance X-ray diffractometer at 40 kV and 40 mA for monochromatized Cu Kα1 (λ = 1.5418 Å) radiation. Morphologies of the prepared samples were further examined with transmission electron microscopy (TEM) by a Hitachi 7700 electron microscope operated at an accelerating voltage of 100 kV. UV–vis diffuse reflectance spectra (DRS) of the samples were measured by using Hitachi U-3010 UV–vis spectrophotometer. Raman spectra were recorded on a Horiba HR 800 spectrometer in the range of 100–1500 cm^{-1}. The excitation light was 514 nm. Chemical characterization of the sample surface was recorded with X-ray photoelectron spectroscopy (XPS ESCALAB 250Xi, Thermo Scientific). The charging effect was calibrated using the binding energy of C1s.

The photocurrent and Mott Schottky measurements were measured on an electrochemical system (CHI-660D, China). The as-prepared samples for the fabrication of photoanode were obtained by mixing 1 mL of ethanol and 10 mg of as-prepared photocatalyst homogeneously. Then the homogeneous mixture was spread on the indium tin oxide (ITO) conducting glass. After the films were dried under ambient conditions, they were sintered in air at 200 °C for 5 h. The photocurrent and Mott Schottky measurements were measured with a standard three-electrode cell with a working electrode (as-prepared photocatalyst films on ITO conducting glass), a platinum wire as counter electrode, and a standard calomel electrode (SCE) as reference electrode. 0.1 M Na_2SO_4 was used as the electrolyte solution. An 11 W ultraviolet germicidal lamp was used as the excitation light source.

2.2. Photocatalytic experiments

The photocatalytic activities were evaluated by the decomposition of MB under UV light (λ = 254 nm, 15 W) irradiation on an XPA photochemical reactor (Xujiang, Nanjing, China). A total of 25 mg of photocatalyst was dispersed in an aqueous solution of MB (50 mL, 0.02 mM). Before irradiation, the suspensions were first ultrasonicated for 10 min and then stirred for 30 min to ensure adsorption–desorption equilibrium between the catalysts and MB. At certain time intervals, 5 mL aliquots were sampled and centrifuged to remove the particles. The concentration of MB was analyzed by recording the absorbance at the characteristic band of 663 nm using a Hitachi U-3010 UV–vis spectrophotometer. The intermediates formed in the degradation process of MB were identified by HPLC (Lumtech) system. Venusil XBP-C_{18} (250 mm × 4.6 mm i.d., 5 μm) reversed phase column was used. The mobile phase consisted of two solutions namely A and B (60:40, v/v) with a flow rate of 1.0 mL min^{-1}. Solution A was made from 0.1 M ammonium acetate and acetic acid (pH 5.3), and solution B was acetonitrile. The UV detector was operated at 292 nm. Total organic carbon analyzer (Multi N/C 2100, Jena) was employed for mineralization degree analysis of MB and phenol solutions.

3. Results and discussion

3.1. Effect of F^- doping on the structure of $BiPO_4$

Fig. 1 showed the XRD patterns of $BiPO_4$ with different fluorine concentrations. The XRD profiles of the $BiPO_4$ and F-$BiPO_4$ samples could be indexed to the pure monoclinic phase (space group $P21/n$, JCPDS 15-0767. a = 6.752 Å, b = 6.933 Å, c = 6.468 Å). The peaks at 27.15°, 29.10°, and 31.22° could be assigned to (2 0 0), (1 2 0) and (0 1 2) crystal planes of monoclinic $BiPO_4$, respectively. Although the crystal phase was not changed by fluorine doping, the relative peak intensities of the (2 0 0), (1 2 0) and (0 1 2) planes were changed. The ratio of 200/120 firstly increased and then decreased

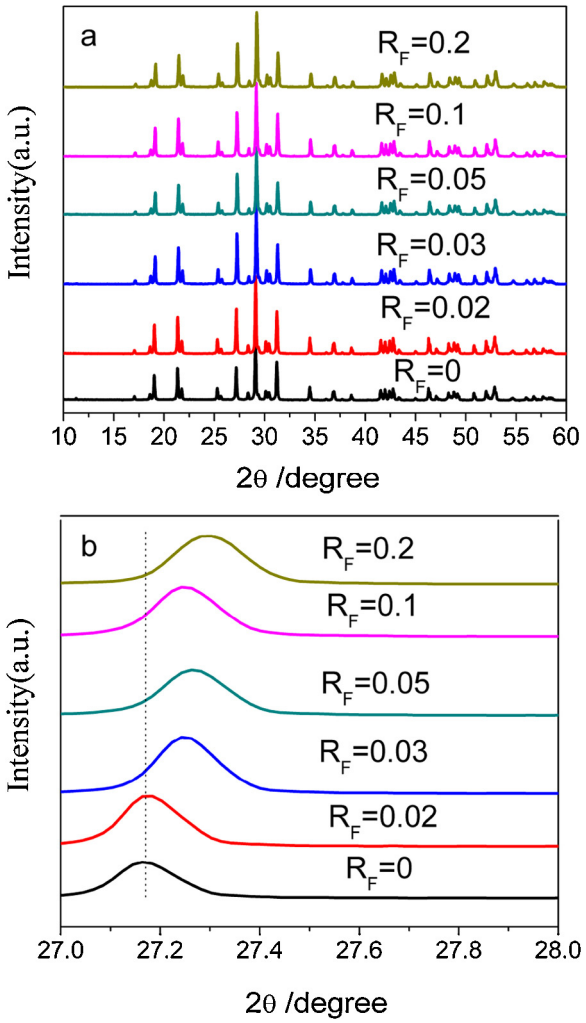

Fig. 1. (a) XRD patterns of $BiPO_4$ and F-$BiPO_4$; (b) diffraction peak positions of the (2 0 0) plane in the range of 2θ = 27.0–28.0°.

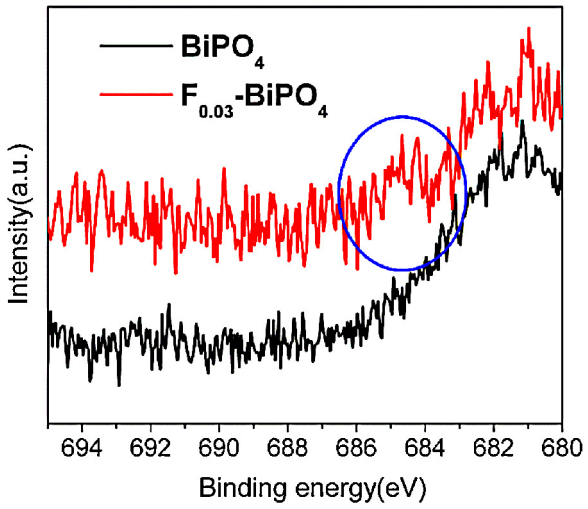

Fig. 2. The XPS spectra of $BiPO_4$ and F-$BiPO_4$ (F1s).

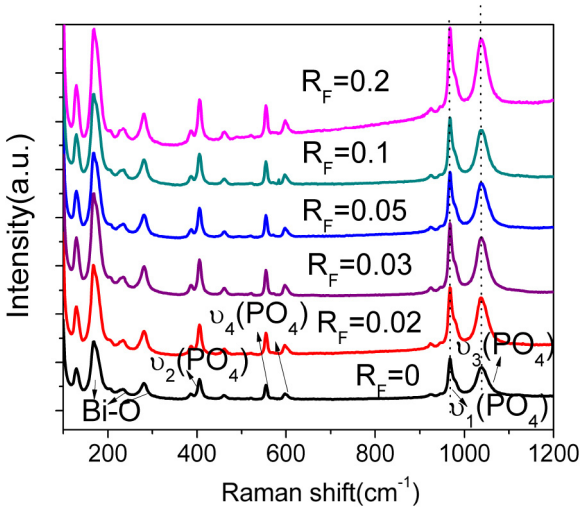

Fig. 3. Raman spectroscopy of $BiPO_4$ and F-$BiPO_4$.

as R_F increased, and it reached the highest value when R_F was 0.03. So $F_{0.03}$-$BiPO_4$ sample had the most obvious preferential crystallographic orientation along the [1 0 0] direction. This was probably caused by the selective adsorption of F^- on certain facet of $BiPO_4$. In addition to the preferential crystallographic orientation, a careful comparison of the (2 0 0) diffraction peak in the range of 27–28° (Fig. 1b) showed that the peak position of $BiPO_4$ with different fluorine contents shifted slightly toward a higher 2θ value. The same results were presented in other diffraction peaks. According to Bragg's law (Eq. (1)),

$$d_{(hkl)} = \frac{n\lambda}{2\sin\theta} \quad (1)$$

where $d_{(hkl)}$ is the distance between crystal planes of ($h\,k\,l$), λ is the X-ray wavelength, and θ is the diffraction angle of the crystal plane ($h\,k\,l$). The increase in 2θ value should result from the decrease in lattice parameters (d (2 0 0) value). The ionic radius of F^- (0.133 nm) is smaller than that of O^{2-} (0.140 nm), and the substitution of O^{2-} by F^- could result in the decrease of d ($h\,k\,l$) value and thus the increase in 2θ values. Therefore, the observed shift of the diffraction peak toward higher angle could be due to the substitution of lattice O by F. The existence of fluorine in F-$BiPO_4$ could also be confirmed by the XPS spectra (Fig. 2), although there was an overlap of F1s and Bi4p XPS spectra.

Fig. 3 showed Raman spectra of $BiPO_4$ with different fluorine concentrations. In all spectra, the observed intense band at 170 cm^{-1} with a shoulder at 231 cm^{-1} corresponds to the Bi—O stretching vibration. The bands centered at 1038 and 970 cm^{-1} are ascribed to the asymmetric ($\nu 3$) and symmetric ($\nu 1$) stretching vibrations of the PO_4 group, respectively. The $\nu 4$ bending vibration modes of PO_4 groups occur at 554 and 596 cm^{-1}, and $\nu 2$ bending vibration occur at 406 and 460 cm^{-1} [9]. The positions of these Raman peaks were not changed but the intensities were increased by fluorine doping. This was also the case for fluorine doped Bi_2WO_6 [24]. The enhanced intensity may be caused by the increased polarizability and crystallinity.

3.2. Effect of F^- doping on the light absorption of $BiPO_4$

The DRS spectra of the $BiPO_4$ and F-$BiPO_4$ samples were recorded to characterize the optical properties (Fig. 4). Fluorine doping obviously affected light absorption characteristics of $BiPO_4$. The absorption spectra of the F-$BiPO_4$ samples showed a slight red shift in the band-gap transition. However, visible light absorption could not be realized by fluorine doping in the range of 0.02–0.2. The absorption above 400 nm confirmed that $F_{0.2}$-$BiPO_4$ possessed the most defects among all the samples.

3.3. Enhancement of photocatalytic activity

The photoactivity of the $BiPO_4$ and F-$BiPO_4$ samples was evaluated by degradation of MB. Fig. 5 showed the relationship between photoactivity and the apparent rate reaction constant (k) of MB degradation over $BiPO_4$ and F-$BiPO_4$. Compared with pure $BiPO_4$, the photocatalytic activity of F-$BiPO_4$ firstly increased then decreased as the fluorine concentration increased from 0.02 to 0.2. The k reached the highest value and it was about 30% higher than the undoped sample when R_F was 0.03. However, further increasing the doped fluorine concentration could decrease the k value and k finally became smaller than that of the undoped sample when R_F was 0.2.

To investigate the degradation process of MB over $BiPO_4$ and F-$BiPO_4$ samples, the composition of MB intermediates were detected by HPLC (Fig. 6). Five peaks were detected from the spectra and they were assigned to MB, azure B(AB), azure A(AA), azure C(AC) and thionin (Th) [34,35]. From these intermediates, it could be concluded that MB was degraded through demethylation by both $BiPO_4$

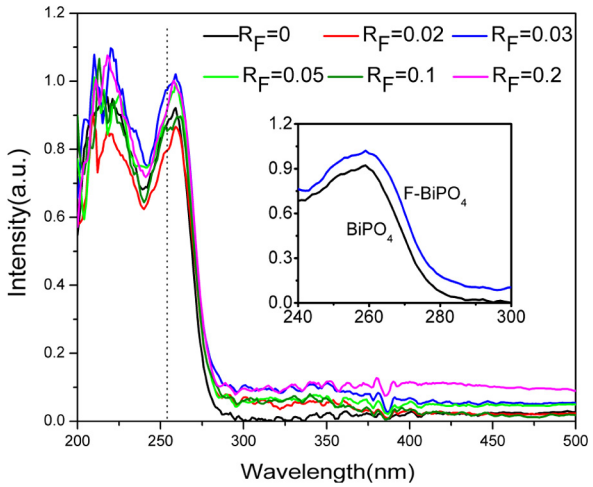

Fig. 4. DRS of $BiPO_4$ and F-$BiPO_4$ (the inset is the magnified figure for the $BiPO_4$ and $F_{0.03}$-$BiPO_4$).

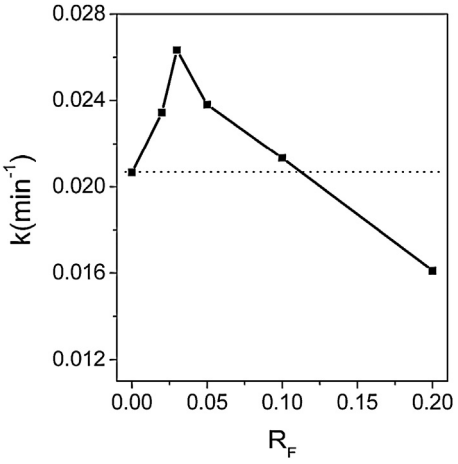

Fig. 5. Apparent rate constant (k) vs R_F.

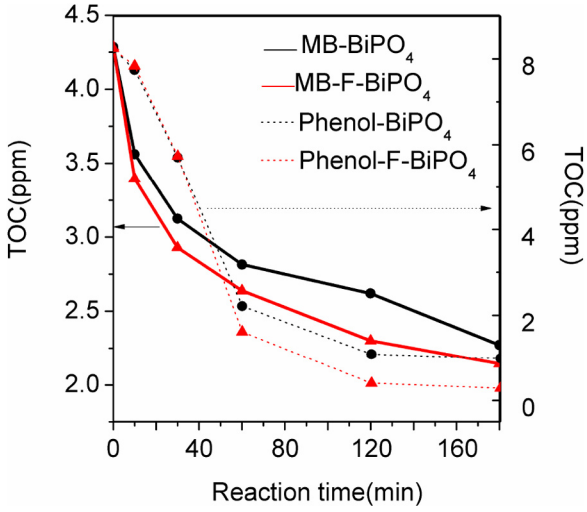

Fig. 7. Changes of TOC during the photocatalytic degradation of MB and phenol over $BiPO_4$ and F-$BiPO_4$ (R_F = 0.03).

and F-$BiPO_4$. Therefore, the degradation pathway of MB was not changed by fluorine doping.

TOC was conducted to elucidate the effects of fluorine on the mineralization ability of $BiPO_4$ photocatalysis. Fig. 7 showed that MB and phenol could be efficiently removed by $BiPO_4$ and F-$BiPO_4$. Therefore, F-$BiPO_4$ was more efficient than $BiPO_4$ in the mineralization of both colored dye and colorless pollutants.

3.4. Mechanism of enhanced photoactivity

There are several key factors influencing the photocatalytic capability of a semiconductor, including the absorption capacity of the incident photons, the photo excitation efficiency of electron-hole pairs, the migration and separation rate of carriers, the redox capabilities of excited-state electrons and holes, as well as the nature of its surface/interface chemistry, which includes the surface energy and chemisorption properties of the photocatalyst [36].

Based on the DRS spectra of $BiPO_4$ and F-$BiPO_4$ samples, the absorption abilities of $F_{0.03}$-$BiPO_4$ and $F_{0.2}$-$BiPO_4$ above 254 nm (the irradiation light wavelength) were similar, whereas the photocatalytic activity of the two samples were the highest and lowest among all the samples, respectively. Besides, $F_{0.02}$-$BiPO_4$ possessed the lowest absorption ability among the other four samples, whereas its photocatalytic activity was almost the highest among them. Thus the absorption capacity of the incident photons and the photo excitation efficiency of electron-hole pairs were not the decisive factors for their photocatalytic activity.

Photocurrent is a direct reflection of the mobility capability of electrons generated in the photocatalyst, and the rate should directly correlate with the photocatalytic activity of the material [37]. Fig. 8 showed the photocurrent of $BiPO_4$ and F-$BiPO_4$ samples generated in suspensions under UV light. It was noted that except for $F_{0.2}$-$BiPO_4$, the photocurrent generated from the fluorine doped $BiPO_4$ were all larger than that of pure $BiPO_4$. The increased photocurrent of F-$BiPO_4$ could be attributed to the higher separation efficiency of photogenerated electron-hole pairs. As for $F_{0.2}$-$BiPO_4$, its relatively low photocurrent might be caused by the fast recombination rate of photogenerated electron-hole pairs [38].

To understand the difference in electronic properties of $BiPO_4$ and F-$BiPO_4$ electrodes, Mott Schottky (MS) measurements (Fig. 9) were performed in the darkness by using the impedance technique. As we know from the classical Mott Schottky theory, when the doping semiconductor space-charge region is depleted as it is under

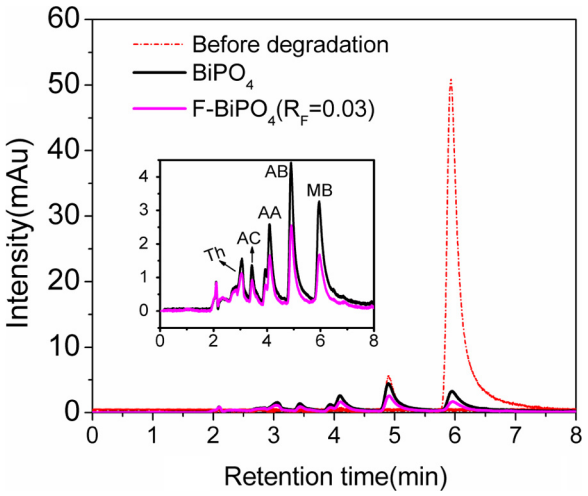

Fig. 6. HPLC spectrum of MB solution before and after photocatalysis (30 min of reaction time) over $BiPO_4$ and F-$BiPO_4$ (R_F = 0.03) (The inset is the magnified figure for the after photocatalysis solutions).

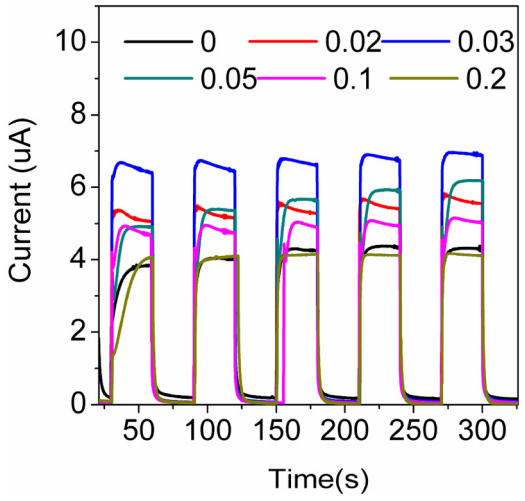

Fig. 8. Photocurrent response for $BiPO_4$ with different R_F.

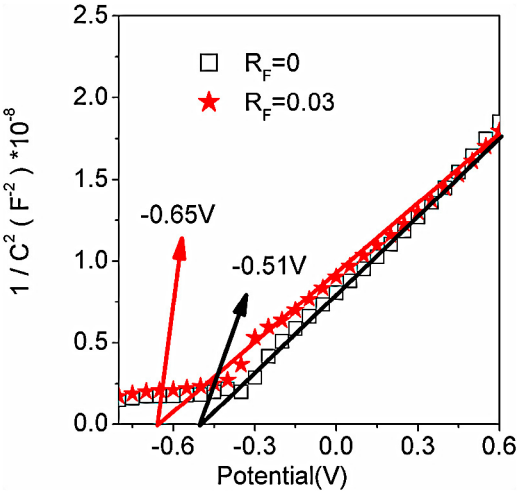

Fig. 9. Mott Schottky (MS) plots of the different catalysts film electrodes.

biasing conditions, the capacitance of space charge region can be described after simplification as Eq. (2)

$$\frac{1}{C^2} = \frac{2}{eN_d\varepsilon_0\varepsilon}\left|V - V_{fb}\right| + \frac{1}{C_H^2} \quad (2)$$

where e is the electronic charge, ε_0 is the permittivity of free space, ε is the dielectric constant of the $BiPO_4$ material, N_d is the dopant (donor or acceptor) concentration, V is the applied potential, V_{fb} is the flat-band potential and C_H is the Helmholtz capacitance of the electrode [39,40]. The flat-band potential V_{fb} can be obtained from the x-intercept of the linear region of the curve $1/C^2$ vs V, and the dopant density N_d can be determined from the slope of the linear region. Based on Fig. 9, the flat-band potential of $BiPO_4$ and F-$BiPO_4$ (R_F 0.03) electrodes were −0.51 V and −0.65 V vs SCE, respectively. It is generally known that the conduction band minimum (CBM) in many n-type semiconductors is more negative by approximately 0.1 V than the flat band potential [41]. Therefore, F-$BiPO_4$ showed a negative shift of the conduction band compared with the pure $BiPO_4$. Based on the band gap (Supporting Information Fig. S1), the estimated positions of valence band maximum (VBM) were 3.29 and 3.03 V vs SCE for $BiPO_4$ and F-$BiPO_4$, respectively. The negative shift of CBM and VBM would be in relation to the increase of the reduction potential of the photogenerated electrons and the decrease of the oxidation potential of holes. However, the lowered oxidation potential of F-$BiPO_4$ was still a little bit higher than or equal to that of TiO_2 (2.9 V vs NHE [42], thus ca. 2.7 V vs SCE), which guaranteed its strong oxidation power for MB and phenol. In addition, the slope of the linear region for F-$BiPO_4$ showed a smaller value than that of $BiPO_4$, indicating higher donor density for the doped electrode. According to photocatalytic mechanism, the higher the donor density for the doped electrode, the faster the photocatalytic degradation rate [29]. This was further proved by the photocurrent. Therefore, the enhancement of photocatalytic activity could be attributed to the higher separation efficiency of electron-hole pairs, and a large number of holes participated in the photocatalytic process caused by fluorine.

In terms of the morphology and structure of the photocatalyst, several factors could influence the separation and recombination efficiency of photogenerated electron-hole pairs. These factors include particle sizes [8], crystallinity [36], dipole moment [43] and defects [38]. Small particle sizes are beneficial to decrease the electron hole migration distance and high crystallinity will reduce electron hole recombination rate. On the basis of XRD, the crystallinity of the samples was fine. Based on TEM (Fig. 10) images of $BiPO_4$ and F-$BiPO_4$, it could be seen that the samples were all nanorods. As for the 1D nanostructure, increasing the aspect ratio (the ratio of length to diameter or surface to volume) generally

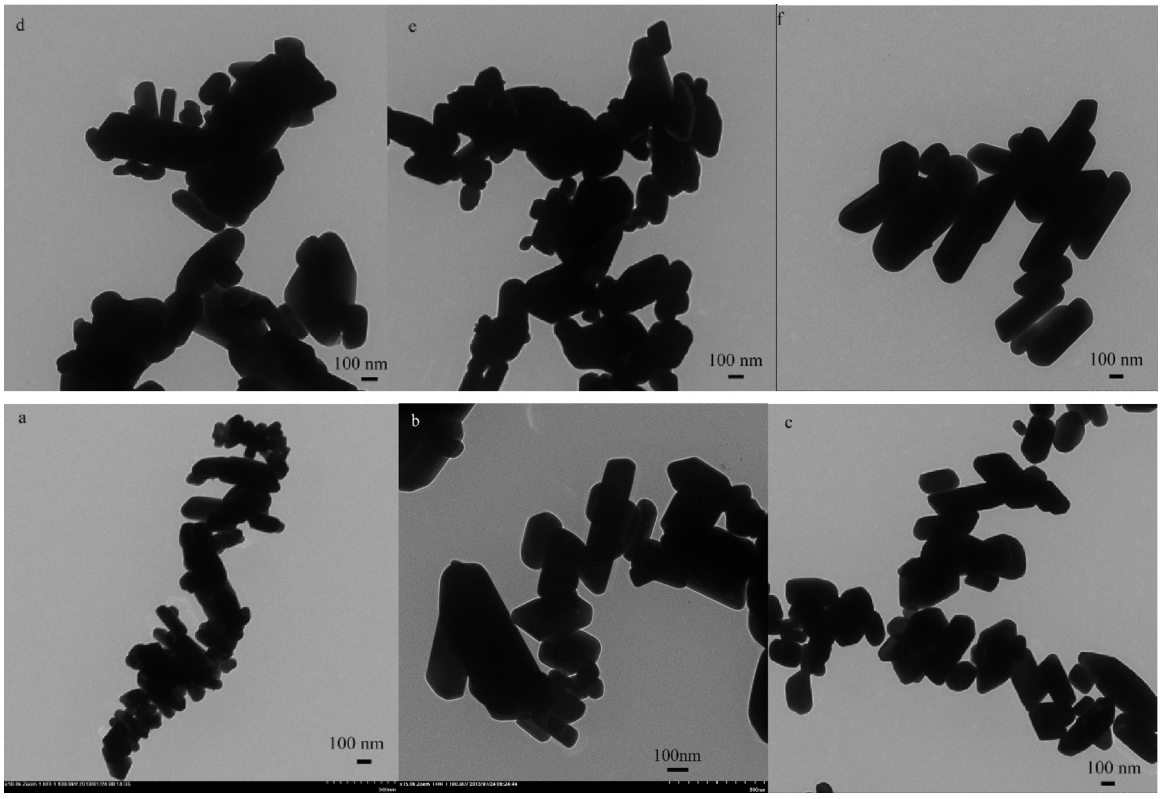

Fig. 10. TEM images of $BiPO_4$ and F-$BiPO_4$. R_F = 0 (a), 0.02 (b), 0.03 (c), 0.05 (d), 0.1 (e), 0.2 (f).

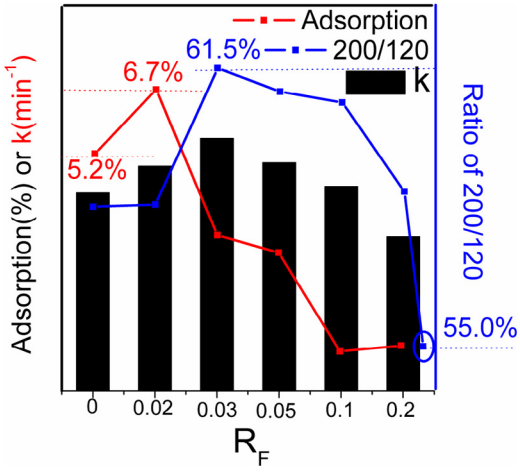

Fig. 11. Adsorption percentage of MB on F-$BiPO_4$ after equilibrium, ratio of 200/120 and the apparent rate constant (k) with different R_F (the point in circle is calculated from JCPDS 15-0767).

results in an enhancement of activity [36]. In our work, $BiPO_4$ samples with different fluorine concentrations possess similar morphology and aspect ratio, except that $F_{0.2}$-$BiPO_4$ had relatively larger aspect ratio. The larger aspect ratio did not result in higher photocatalytic activity. On the contrary, $F_{0.2}$-$BiPO_4$ had the lowest activity. Therefore, particle size was not the decisive factor for the photocatalytic activity. Raman spectra revealed that the polarizability could be increased by F-doping. The increased polarizability would increase the induced dipole moment and thus increase separation efficiency of photogenerated electron-hole pairs. Thus the increased polarizability was partly responsible for the increased photocatalytic activity. It could be concluded from the DRS that there were the most defects in $F_{0.2}$-$BiPO_4$. It is stated that defects form the trapping centers of photoinduced electrons and holes at low defect concentration and change to recombination centers at high defect concentration [38]. In our case, the high concentration defect induced by fluorine doping resulted in fast recombination rate of photogenerated electron-hole pairs and thus low photocatalytic activity. To conclude, the separation and recombination rates of photogenerated electron-hole pairs were mainly mediated by the induced dipole moment and defects by F-doping.

Apart from the above factors, the nature of photocatalyst's surface/interface chemistry is another dominating factor influencing the photocatalytic capability of a photocatalyst. In general, a stronger adsorption ability of the substrate [44,45] and larger percentage of highly reactive facets will yield higher photocatalytic activity [46–49]. As for the fluorine doped $BiPO_4$, adsorption played an important role on their photocatalytic activity. Based on Fig. 11, it was clear that the adsorption of MB on $BiPO_4$ was altered by fluorine doping. Compared with $BiPO_4$, the amount of MB adsorbed on F-$BiPO_4$ firstly increased then deceased as the fluorine concentration increased from 0.02 to 0.2. The plateau was reached when R_F was 0.02. When R_F increased to 0.2, the adsorption content decreased to 1/5 of the pure $BiPO_4$. This result might seem strange at first glance and one might even doubt whether the adsorption-desorption equilibrium had been achieved. To clarify this question, we examined the change of adsorption percentage over time in dark and found that the percentage of MB adsorbed on $BiPO_4$ at 30 min and 90 min were similar, and the relationship between adsorption percentage and R_F was the same. The "first increase then decease" phenomenon was speculated to be related with the state of fluorine in $BiPO_4$. When the amount of added fluoride was small, most of the fluoride was adsorbed on the surface of $BiPO_4$, making the photocatalyst more negative. MB molecule, as a cationic dye, would be much easier to be adsorbed on the negative surface. When the amount of added fluoride increased, most of the F^- went deep into the lattice of $BiPO_4$, substituted the lattice O^{2-} and made the surface of $BiPO_4$ less negative. Thus, the cationic MB molecule would be less likely to adsorb on such surfaces. The adsorption ability of F-$BiPO_4$ had some correlation with the photocatalytic activity. In general, the stronger the adsorption ability was, the higher the photocatalytic activity became. However, there also existed some exceptional cases. The low adsorption ability of $F_{0.03}$-$BiPO_4$ did not result in low photocatalytic activity. Besides, $F_{0.1}$-$BiPO_4$, possessing similar or even lower adsorption ability for MB than $F_{0.2}$-$BiPO_4$, had higher photocatalytic activity than $F_{0.2}$-$BiPO_4$. Furthermore, it could be seen that the maximum amount of MB adsorbed on F-$BiPO_4$ was less than 10%. This small value indicated that adsorption ability could not be the decisive factor for the high photocatalytic activity of F-$BiPO_4$. In general, a higher surface energy yields higher catalytic activity. So much effort has been made in synthesizing photocatalysts with highly reactive facets. Based on the XRD, it can be seen that the ratio of 200/120 had some correlation with the photocatalytic activity. When R_F was in the range of 0–0.05, the larger the ratio of 200/120 became, the higher the photocatalytic activity was. So there must be more active facets when $BiPO_4$ nanorods grow along the [1 0 0] direction. The larger amount of active facets would contribute to the enhanced photocatalytic activity of F-$BiPO_4$.

4. Conclusion

The photocatalytic activity of $BiPO_4$ could be improved by F-doping. This could be attributed to the stronger adsorption ability of the substrate, the larger amount of active facet and higher separation efficiency of electron-hole pairs. The photocatalytic process would be inhibited by high dopant concentration ($\geq$0.2) due to the increased recombination rate of electron-hole pairs at high defect concentration. Although a red shift of the optical absorption edge of $BiPO_4$ was induced by F-doping, visible light absorption cannot be achieved.

Acknowledgments

This work was partly supported by National Basic Research Program of China (973 Program) (2013CB632403), National High Technology Research and Development Program of China (2012AA062701), Chinese National Science Foundation (20925725 and 21373121), and Special Project on Innovative Method from the Ministry of Science and Technology of China (2012 IM030500).

Appendix A. Supplementary data

Supplementary material related to this article can be found, in the online version, at http://dx.doi.org/10.1016/j.apcatb.2013.09.050.

References

[1] C. Pan, Y. Zhu, Environmental Science & Technology 44 (2010) 5570–5574.
[2] Y. Liu, X. Ma, X. Yi, Y. Zhu, Acta Physico-Chimica Sinica 28 (2012).
[3] C.C. Fu, G.S. Li, M.L. Zhao, L.S. Yang, J. Zheng, L.P. Li, Inorganic Chemistry 51 (2012) 5869–5880.
[4] G. Li, Y. Ding, Y. Zhang, Z. Lu, H. Sun, R. Chen, Journal of Colloid and Interface Science 363 (2011) 497–503.
[5] B. Lu, X. Ma, C. Pan, Y. Zhu, Applied Catalysis A-General 435 (2012) 93–98.
[6] C. Pan, J. Xu, Y. Chen, Y. Zhu, Applied Catalysis B-Environmental 115 (2012) 314–319.
[7] C. Pan, J. Xu, Y. Wang, D. Li, Y. Zhu, Advanced Functional Materials 22 (2012) 1518–1524.
[8] C. Pan, Y. Zhu, Journal of Materials Chemistry 21 (2011) 4235–4241.
[9] M. Zhao, G. Li, L. Li, L. Yang, J. Zheng, Crystal Growth & Design 12 (2012) 3983–3991.

[10] Y. Liu, Y. Zhu, J. Xu, X. Bai, R. Zong, Y. Zhu, Applied Catalysis B-Environmental 142–143 (2013) 561–567.
[11] R. Asahi, T. Morikawa, T. Ohwaki, K. Aoki, Y. Taga, Science 293 (2001) 269–271.
[12] Y.X. Niu, M.Y. Xing, J.L. Zhang, B.Z. Tian, Catalysis Today 201 (2013) 159–166.
[13] J.L. Zhang, Y.M. Wu, M.Y. Xing, S.A.K. Leghari, S. Sajjad, Energy & Environmental Science 3 (2010) 715–726.
[14] X. Chen, S.S. Mao, Chemical Reviews 107 (2007) 2891–2959.
[15] F. Dong, H. Wang, Z. Wu, Journal of Physical Chemistry C 113 (2009) 16717–16723.
[16] O. Diwald, T.L. Thompson, T. Zubkov, E.G. Goralski, S.D. Walck, J.T. Yates, Journal of Physical Chemistry B 108 (2004) 6004–6008.
[17] Y. Izumi, T. Itoi, S. Peng, K. Oka, Y. Shibata, Journal of Physical Chemistry C 113 (2009) 6706–6718.
[18] N.O. Gopal, H.H. Lo, T.F. Ke, C.H. Lee, C.C. Chou, J.D. Wu, S.C. Sheu, S.C. Ke, Journal of Physical Chemistry C 116 (2012) 16191–16197.
[19] G.Z. Shen, J.H. Cho, J.K. Yoo, G.C. Yi, C.J. Lee, Journal of Physical Chemistry B 109 (2005) 5491–5496.
[20] G. Liu, P. Niu, C. Sun, S.C. Smith, Z. Chen, G.Q. Lu, H.M. Cheng, Journal of the American Chemical Society 132 (2010) 11642–11648.
[21] G. Huang, R. Shi, Y. Zhu, Journal of Molecular Catalysis A-Chemical 348 (2011) 100–105.
[22] G. Huang, Y. Zhu, Journal of Physical Chemistry C 111 (2007) 11952–11958.
[23] D. Li, H. Haneda, S. Hishita, N. Ohashi, N.K. Labhsetwar, Journal of Fluorine Chemistry 126 (2005) 69–77.
[24] R. Shi, G. Huang, J. Lin, Y. Zhu, Journal of Physical Chemistry C 113 (2009) 19633–19638.
[25] J.G. Yu, W.G. Wang, B. Cheng, B.L. Su, Journal of Physical Chemistry C 113 (2009) 6743–6750.
[26] X.T. Hong, Z.P. Wang, W.M. Cai, F. Lu, J. Zhang, Y.Z. Yang, N. Ma, Y.J. Liu, Chemistry of Materials 17 (2005) 1548–1552.
[27] D. Li, H. Haneda, N.K. Labhsetwar, S. Hishita, N. Ohashi, Chemical Physics Letters 401 (2005) 579–584.
[28] J.C. Yu, J.G. Yu, W.K. Ho, Z.T. Jiang, L.Z. Zhang, Chemistry of Materials 14 (2002) 3808–3816.
[29] G. Huang, S. Zhang, T. Xu, Y. Zhu, Environmental Science & Technology 42 (2008) 8516–8521.
[30] S. Chen, S. Sun, H. Sun, W. Fan, X. Zhao, X. Sun, Journal of Physical Chemistry C 114 (2010) 7680–7688.
[31] J.S. Wang, Y. Shu, Q.W. Zhang, F. Saito, T. Sato, Solid State Ionics 172 (2004) 191–195.
[32] J.S. Park, W. Choi, Langmuir 20 (2004) 11523–11527.
[33] M.Y. Xing, D.Y. Qi, J.L. Zhang, F. Chen, B.Z. Tian, S. Bagwas, M. Anpo, Journal of Catalysis 294 (2012) 37–46.
[34] M.A. Rauf, M.A. Meetani, A. Khaleel, A. Ahmed, Chemical Engineering Journal 157 (2010) 373–378.
[35] C. Yogi, K. Kojima, N. Wada, H. Tokumoto, T. Takai, T. Mizoguchi, H. Tamiaki, Thin Solid Films 516 (2008) 5881–5884.
[36] H. Tong, S.X. Ouyang, Y.P. Bi, N. Umezawa, M. Oshikiri, J.H. Ye, Advanced Materials 24 (2012) 229–251.
[37] H.G. Kim, P.H. Borse, W.Y. Choi, J.S. Lee, Angewandte Chemie-International Edition 44 (2005) 4585–4589.
[38] B.S. Liu, K. Nakata, X.J. Zhao, T. Ochiai, T. Murakami, A. Fujishima, Journal of Physical Chemistry C 115 (2011) 16037–16042.
[39] F. Fabregat-Santiago, G. Garcia-Belmonte, J. Bisquert, P. Bogdanoff, A. Zaban, Journal of the Electrochemical Society 150 (2003) E293–E298.
[40] W. Geng, W. Qiang, L. Wu, L. Jinghong, Journal of Physical Chemistry B 110 (2006) 22029–22034.
[41] Y. Matsumoto, Journal of Solid State Chemistry 126 (1996) 227–234.
[42] Y. Xu, M.A.A. Schoonen, American Mineralist 85 (2000) 543–556.
[43] J. Sato, H. Kobayashi, Y. Inoue, Journal of Physical Chemistry B 107 (2003) 7970–7975.
[44] Q. Wang, C. Chen, D. Zhao, W. Ma, J. Zhao, Langmuir 24 (2008) 7338–7345.
[45] Y.H. Zhang, Z.R. Tang, X.Z. Fu, Y.J. Xu, ACS Nano 4 (2010) 7303–7314.
[46] X. Han, Q. Kuang, M. Jin, Z. Xie, L. Zheng, Journal of the American Chemical Society 131 (2009) 3152–3513.
[47] H.G. Yang, G. Liu, S.Z. Qiao, C.H. Sun, Y.G. Jin, S.C. Smith, J. Zou, H.M. Cheng, G.Q. Lu, Journal of the American Chemical Society 131 (2009) 4078–4083.
[48] F. Tian, Y. Zhang, J. Zhang, C. Pan, Journal of Physical Chemistry C 116 (2012) 7515–7519.
[49] Y. Luan, L. Jing, Y. Xie, X. Sun, Y. Feng, H. Fu, ACS catalysis 3 (2013) 1378–1385.